

# Nanoscale

Accepted Manuscript



This is an *Accepted Manuscript*, which has been through the Royal Society of Chemistry peer review process and has been accepted for publication.

*Accepted Manuscripts* are published online shortly after acceptance, before technical editing, formatting and proof reading. Using this free service, authors can make their results available to the community, in citable form, before we publish the edited article. We will replace this *Accepted Manuscript* with the edited and formatted *Advance Article* as soon as it is available.

You can find more information about *Accepted Manuscripts* in the [Information for Authors](#).

Please note that technical editing may introduce minor changes to the text and/or graphics, which may alter content. The journal's standard [Terms & Conditions](#) and the [Ethical guidelines](#) still apply. In no event shall the Royal Society of Chemistry be held responsible for any errors or omissions in this *Accepted Manuscript* or any consequences arising from the use of any information it contains.

# Exchange-biased hybrid ferromagnetic-multiferroic core-shell nanostructures<sup>†</sup>

Da-Wei Shi,<sup>a</sup> Khalid Javed,<sup>a</sup> Syed Shahbaz Ali,<sup>a</sup> Jun-Yang Chen,<sup>a</sup> Pei-Sen Li,<sup>b</sup> Yong-Gang Zhao<sup>b</sup> and Xiu-Feng Han<sup>\*a</sup>

Received Xth XXXXXXXXXXXX 20XX, Accepted Xth XXXXXXXXXXXX 20XX

First published on the web Xth XXXXXXXXXXXX 200X

DOI: 10.1039/b000000x

**Artificial exchange-biased two-phase core-shell nanostructures consisting of ferromagnetic (Ni) and multiferroic (BiFeO<sub>3</sub>) materials were manufactured by a two-step method. Exchange bias effect was observed and studied, which indicates that it is possible to fabricate ferromagnetic-multiferroic nanostructures to utilize the combined ferroelectric and antiferromagnetic functionalities of bismuth ferrite.**

Coaxial nanostructures, which may exhibit additional effects and have potential applications as multi-function materials, have attracted considerable attention both for fundamental and technological interest.<sup>1–4</sup> Compared with the single-phase nanomaterials, such hybrid nanostructures with a combination of two or more components may show enhanced properties or offer multifunctional properties. Up to now, various methods have been developed to synthesize these coaxial nanostructures. Among them, template-assisted technique can be easily integrated with other methods such as electrochemical deposition,<sup>5,6</sup> sol-gel,<sup>7</sup> atomic layer deposition (ALD),<sup>8</sup> supercritical fluids (SCF)<sup>9</sup> and chemical vapor deposition (CVD)<sup>10</sup> for the preparation of numerous functional nanomaterials. Moreover, easily controllable morphologies of the nanostructures makes the low-cost template-assisted technique one of the most commonly used method for the fabrication of one-dimensional (1D) coaxial nanostructures.

It has been proven that magnetic and ferroelectric order can coexist in some unusual perovskite-type oxide materials, termed as multiferroics.<sup>11,12</sup> Multiferroics have attracted great interest due to their potential applications in novel nonvolatile information storages and new magnetoelectric sensors by a combination of ferroelectric and ferromagnetic

properties. Though a number of materials have been demonstrated to be multiferroic, BiFeO<sub>3</sub> (BFO) with a ferroelectric Curie temperature of 1100 K and an antiferromagnetic Neel temperature of 640 K seems to be the most promising candidate among the materials studied.<sup>13,14</sup> Investigations on this rhombohedral perovskite started since the late 1950s in the bulk form.<sup>15</sup> Researchers around the world paid endlessly efforts on the studies of physical and structural properties of BFO since then. Recently, Wang et al. reported on the growth and properties of thin epitaxial BFO films triggered new research enthusiasm for the study of BFO thin films.<sup>16</sup> To the best of our knowledge, only few works have been done on the synthesis of the BFO 1D nanostructure to date.<sup>17,18</sup> In addition, proper synthesis conditions and structure characterization of 1D BFO nanostructure is still controversial based on the limited works done by other researchers. Due to the rather weak net magnetic moment of the BFO, the use of artificial two-phase systems consisting of ferromagnetic materials and BFO, serves as an alternative approach to utilize the combined ferroelectric and antiferromagnetic functionalities of bismuth ferrite. Thin films consisting of ferromagnetic materials and BFO have been widely studied in recent years.<sup>19,20</sup> However, no related works on the hybrid 1D nanostructures has been carried out so far. Another exciting area in materials science nowadays is the study of ferromagnetic nanostructures such as nanowires and nanotubes. Due to their potential applications in ultrahigh magnetic recording media, ultra-small magnetic sensor, drug delivery etc.,<sup>21,22</sup> we have continuously carried out research on the structural and magnetic properties of ferromagnetic nanotube/nanowire arrays consisting of elemental Fe, Co, Ni, as well as their alloys during the past few years.<sup>23,24</sup>

In this work, we reported the fabrication of well-ordered hybrid ferromagnetic-multiferroic core-shell nanostructures. Ferromagnetic metal Ni and bismuth ferrite serve as the core and shell of the coaxial nanostructures, respectively. We have studied the magnetic properties and magnetic reversal mechanism of the ferromagnetic-multiferroic core-shell

<sup>a</sup> Beijing National Laboratory for Condensed Matter Physics, Institute of Physics, Chinese Academy of Sciences, Beijing 100190, China. E-mail: xfhan@aphy.iphy.ac.cn

<sup>b</sup> Department of Physics and State Key Laboratory of Low-Dimensional Quantum Physics, Tsinghua University, Beijing 100084, China.

<sup>†</sup> Electronic Supplementary Information (ESI) available. See DOI: 10.1039/b000000x/

nanostructures as well. Furthermore, we have discussed on the exchange bias effect which result from the exchange coupling between the ferromagnetic core and the antiferromagnetic BFO shell. In view of these results, its possible to utilize the combined ferroelectric and antiferromagnetic functionalities of BFO for future new multiferroic devices.

Unique anodic aluminum oxide (AAO) templates with self-assembled hexagonally arranged nanopores are ideal templates for the fabrication of nanoscale materials because of their facile preparation and controllable pore size. Nanowires/nanotubes of metals, conductive polymers, semiconductors, carbon, and composite materials have been fabricated successfully. By using a two-step anodization method, we can fabricate quasi-hexagonal ordered and uniform AAO templates with a wide range of diameters and lengths. Here, porous alumina membranes with two different pore diameters of 120 nm and 300 nm were used for the synthesis of Ni-BFO core-shell nanostructures (Characterizations of the AAO template are shown in the Electronic Supplementary Information). Fig.1 illustrates the synthesis process in detail. First, BFO nanotubes were prepared via template-assisted sol-gel method. Then electrodeposition of Ni nanowires/nanotubes was performed after the single phase perovskite crystal structural BFO shell was obtained.

The phase diagram of bismuth ferrite indicates that unexpected crystallite phases other than BiFeO<sub>3</sub> might be unintentionally induced during the synthesis process.<sup>25</sup> The synthesis of phase pure and stoichiometric bismuth ferrite is challenging mainly because of the volatility of bismuth and other more stable competing phase. To compensate the evaporation during high temperature annealing, appropriate amount of excess bismuth was added for the preparation of sol. Thickness of the nanotubes varied with the time of template dipped into the sol. It has been found that 15 min is enough for the formation of well-ordered and uniform nanotubes while porous nanostructures formed if the infiltration of the precursor is not sufficient (Figure S2). Furthermore, annealing temperature was optimized to obtain a single phase perovskite crystal structure. Templates containing the precursors were annealed at 500°C, 600°C and 700°C respectively. Fig. 2c shows the X-ray diffraction (XRD) patterns of the nanotubes after the templates were dissolved. Clear diffraction peaks were observed for all of the samples. The standard XRD pattern of BiFeO<sub>3</sub> (JCPDS # 20-0169) was also shown for comparison. The nanotubes annealed at 600°C is the one with the least secondary phases. Obvious diffraction peaks from the samples annealed at 500°C and 700°C indicate the existence of second phase Bi<sub>2</sub>Fe<sub>4</sub>O<sub>9</sub> (Figure S3). The XRD patterns of the samples annealed at 500°C and 700°C further confirm that volatility of bismuth and other more stable competing phase are the obstacles for the synthesis of high

quality BiFeO<sub>3</sub> nanomaterials. By adding appropriate amount of excess bismuth and optimizing the annealing temperature, the unexpected second phase can be eliminated. The above experimental results provide convincing evidence for the formation of single phase perovskite BiFeO<sub>3</sub> nanotubes prepared by template-assisted sol-gel method. Fig. 2b shows the surface profile of the AAO template filled with BFO nanotubes obtained by Atomic force microscopy (AFM). Even for the template with a pore diameter of 120 nm, it still maintains the structure of quasi-hexagonal ordered nanopore arrays. Fig. 2d shows the standard bipolar *P-E* hysteresis loop of the BFO nanotubes as grown in AAO template. Measurements were performed with frequency of 200 Hz at room temperature, giving a typical ferroelectric characteristic of the nanotubes. The remnant polarization *P<sub>r</sub>* and the coercive electric field *E<sub>c</sub>* obtained from the *P-E* hysteresis loop are about 26 C/cm<sup>2</sup> and 60 kV/cm, respectively.

Fig. 3 shows the morphology of the BiFeO<sub>3</sub> nanotubes characterized by scanning electron microscope (SEM) and transmission electron microscope (TEM). The diameters and lengths for all of nanotubes are consistent with the diameters of the AAO channel and the thickness of the template respectively. BFO nanotubes were of polycrystalline structure as shown by the HRTEM image (Fig. 3c). To confirm the composition of the nanotubes, Energy dispersive spectrum (EDS) is shown in Fig. 3d. The ratio of Bi:Fe is exactly 1:1, which serve as another evidence for the composition of the BFO nanotubes obtained. It should be pointed out that some other elements also present besides Bi, Fe, and O in the spectrum. The Cu peak originates from copper tape used for the SEM; the Al peak is observed due to the incomplete removal of AAO template. The magnetic properties of BFO nanotubes were investigated by vibrating sample magnetometer (VSM) at room temperature to avoid the influence of the remanence in a superconducting magnet in a SQUID magnetometer. Since BFO is antiferromagnetic at room temperature and the weak local canting moment being completely cancelled by the averaging effect, no ferromagnetism was observed in our hysteresis measurement (Figure S4).

AAO template with pore size of 300 nm filled with BFO nanotubes were used for the electrodeposition of Ni nanotubes/nanowires. Fig. 4a and 4b illustrate the SEM and TEM images of the Ni-BFO core-shell nanotubes with fine and smooth morphologies. The wall thickness of BFO nanotubes is about 20 nm, which is comparable with the thickness of electrodeposited Ni nanotubes. Fig. 4c and 4d clearly show the SEM results of Ni-BFO core-shell nanowires grown in AAO template with pore size of 300 nm. Nanowires with such a huge diameter are inappropriate for TEM characterization, since it is much larger than the

penetration depth of electron (Figure S5). More importantly, it is almost impossible to identify the influence of the thin BFO shell act on the Ni core nanowires. Therefore, we also fabricated the Ni-BFO core-shell nanowires generated from nanopores with diameter of 120 nm. Fig. 5 shows the SEM, TEM and EDS for the Ni-BFO core-shell nanowires with smaller diameter. Fine core-shell structure was observed both from the SEM and TEM images.

Hybrid multiferroic nanostructure (BTO-Co) reported by Narayanan et al demonstrates the existence of magnetoelectric coupling via magnetocapacitance measurements, indicating the possible tunability of the dielectric permittivity with external magnetic field.<sup>4</sup> Here, one-dimensional nanostructures consisting of a ferromagnetic layer in contact with the multiferroics BFO layer are fabricated and the coupling between them has been exploited from another point of view. The antiferromagnetic order of the BFO can be used to establish exchange bias in the hybrid nanostructures,<sup>19</sup> which leads to possible modification in ferromagnetic magnetization through exchange bias effect. More importantly, the magnetoelectric (ME) coupling may realize the reversal of ferroelectric polarization by a magnetic field or the control of magnetism by an electric field. Magnetic properties of Ni-BFO core-shell nanostructures are investigated and shown in Figure 6 and Figure 7.

Fig. 6a shows typical hysteresis loops of Ni-BFO core-shell nanotubes with diameter of 300 nm for magnetic fields applied parallel and perpendicular to the nanotube axis measured at room temperature. As can be seen from the large difference of the loop squareness, the easy axis is perpendicular to the nanotubes axis. The anisotropic field of the nanotubes is mainly determined by three contributions: (1) the shape anisotropy field which tend to induce a magnetic easy axis parallel to the nanotube axis; (2) magnetostatic dipole interaction field which will induce a magnetic easy axis perpendicular to the nanotube axis; (3) magnetocrystalline anisotropy field.<sup>23</sup> Our previous investigations on the ferromagnetic nanotubes have shown that the magnetocrystalline anisotropy field can be neglected since the nanotubes fabricated by electrodeposition method are usually polycrystalline or amorphous. The easy axis is oriented perpendicular to the nanotubes which is similar to our previous results.<sup>24</sup> Exchange interaction at the interface is assumed as the origin of unidirectional anisotropy and exchange bias in the AFM-FM heterostructures. Here, an obvious enhanced coercivity and loop shift has been observed for both directions, which originate from exchange-bias coupling. It should be pointed out that the exchange bias was established without any magnetic-field-annealing process in our experiments. One possible reason for such behavior is

the rearrangement of antiferromagnetic domains during the electrodeposition of Ni nanotubes inside the shell.<sup>19</sup> The angular dependence of coercivity and exchange bias field of Ni-BFO core-shell nanotubes are shown in Fig. 6b ( $\theta$  is the angle between external magnetic field and nanotube axis). The coercivity first increases to a peak value at  $10^\circ$ , followed by a decline to minimum at  $90^\circ$ . Three different types of reversal modes have been proposed to investigate the angular dependence of the coercivity: coherent, curling and nucleation.<sup>24,26</sup> It should be pointed out that coherent mode is only suitable for the short nanotubes. In our case, length of the Ni nanotubes is in the range of a few micrometers. Thus a transition from curling to nucleation mode for the Ni-BFO core-shell nanotubes as the field moves to high angles was used to interpret the magnetization reversal mechanism. Geometry of the nanotubes/nanowires exhibits a great impact on the magnetization reversal mechanism. Since diameter of the Ni nanotubes is much larger than the critical diameter, coercivity increases with the increase of the angle according to the curling mode at small angles. At large field angles, magnetization reversal will take place by nucleation. Angular dependence of exchange bias field shows a similar tendency with a peak at the same angle. Though higher  $H_{ex}$  values were usually observed along the easy axis of magnetization of ferromagnetic materials,<sup>27,28</sup> exchange bias field reaches the maximum value when the magnetic field was along the nanotubes, which is the hard axis in our case. Since the magnetic anisotropy, interface roughness, spin configuration and magnetic/antiferromagnetic domains can all exhibit significant effects on the exchange interaction, the experimental results can be attributed to the microstructure in the distinct crystalline orientations of both the Ni nanotube walls and the BFO shell layer.<sup>29</sup> Fig. 6c shows the hysteresis loops of Ni-BFO core-shell nanotubes at different temperatures (100 K, 120 K, 150 K, 180 K and 300 K). Both the saturation magnetization ( $M_s$ ) and saturation field ( $H_s$ ) increase at lower temperatures, which can be attributed to the large surface/volume ratio and the existence of superparamagnetic nanoparticle.<sup>30</sup> Temperature dependence of coercivity and exchange bias field was illustrated in Fig. 6d,  $H_c$  slightly increases as the temperature decreases, which can be explained by thermal activation over the energy barrier.<sup>31</sup> To exclude possible exchange bias arising from partial natural oxidation of Ni nanotubes,<sup>29</sup> single phase Ni nanotubes were deposited and left in the air for more than two months. Hysteresis loops with magnetic fields applied parallel and perpendicular were measured while no loop shift was seen (Figure S6). Hence it is reasonable to ignore the impact from the probable natural oxidation of the Ni nanotubes.

For the Ni-BFO core-shell nanowires generated from templates with diameter of 300 nm, magnetic properties

similar to single phase Ni nanowires have been found (Figure S7). No exchange bias was observed. We attribute this experimental result to the great disparity of the thickness between the thick ferromagnetic core nanowires and the thin BFO shell. Such experimental results were consistent with the rule of  $H_{ex} \propto t^{-1}$ .<sup>32</sup> Fig. 7a shows the hysteresis loops of Ni-BFO core-shell nanowires fabricated from templates with diameter of 120 nm with magnetic fields applied parallel and perpendicular to the nanowire axis at room temperature. The easy axis orients along the nanowires due to the strong shape anisotropy. An obvious loop shift was observed for both directions, the exchange bias fields were 9 Oe and 15 Oe. The observation of exchange bias and enhanced coercivity can be correlated with the presence of uncompensated spins at the interface between the ferromagnetic core and the antiferromagnetic shell. Fig. 7b shows the angular dependent coercivity and exchange bias field. Different from the nanotubes where a transition from a curling to nucleation mode reversal mechanism exists, the coercivity decreases monotonously with the angle increases, which indicates the dominance of nucleation mode in the magnetization reversal process. The wall thickness of the nanotubes can strongly affect the mechanism of magnetization reversal and the overall magnetic behavior, while for magnetic nanowires the magnetization reversal mechanism depends upon the diameter of the nanowires. Exchange bias field reaches the maximum value when the magnetic field was along the nanowires, which is the hard axis. It can be mainly attributed to the spin structure at the interface and the microstructure of both the Ni nanowires and the BFO shell layer.

## Conclusions

A detailed study on the synthesis of bismuth ferrite nanostructures through template-assisted sol-gel method is presented. Volatility of bismuth and presence of other more stable competing phase are main obstacles for the fabrication of high quality BiFeO<sub>3</sub> nanomaterials. We demonstrate that, by choosing appropriate sol and optimizing the heat treatment conditions, it is possible to grow well-ordered BiFeO<sub>3</sub> nanotubes with the diameter range from 120 nm to 300 nm. Characterizations on the ferroelectric and magnetic properties confirm the coexistence of spontaneous electric polarization and antiferromagnetic spin ordering in the BiFeO<sub>3</sub> nanomaterials. In addition, further deposited ferromagnetic nanowires/nanotubes lead to the formation of ferromagnetic-multiferroic core-shell nanostructures. Though the existence of Bi<sub>2</sub>Fe<sub>4</sub>O<sub>9</sub> as well as the rough core/shell interfaces could reduce the exchange bias effect of the samples, obvious exchange bias was found in the Ni-BFO core-shell nanostructures without any magnetic-field-annealing process. It is

attributed to the rearrangement of the antiferromagnetic domains during the electrodeposition of Ni nanowires/nanotubes inside the BFO shell. Thus we experimentally demonstrated that ferromagnetic cores are exchange-coupled to the multiferroic BFO shell. Ferromagnetic/Ferroelectric two phase 1D nanomaterials with electric-field control of magnetization or magnetic-field control of polarization may be realized. The synthetic methods presented in this work can be easily expanded to the fabrication of other similar heterogeneous nanostructures, which offers new insights into the template synthesized materials at nanoscale in general.

## Acknowledgments

This work was supported by the State Key Project of Fundamental Research of Ministry of Science and Technology [MOST, No.2010CB934400] and National Natural Science Foundation [NSFC, Grant No. 11374351], and the partial support of NSFC-JSPS Scientific Cooperation Program.

## References

- 1 J. L. Lauhon, M. S. Gudixsen, D. Wang, C. M. Lieber, *Nature*, 2002, **420**, 57.
- 2 R. Yan, D. Gargas, P. Yang, *Nature photonics*, 2009, **3**, 569.
- 3 D. Moore, J. R. Morber, R. L. Snyder, Z. L. Wang, *J. Phys. Chem. C*, 2008, **112**, 2895.
- 4 T. N. Narayanan, B. P. Mandal, A. K. Tyagi, A. Kumarasiri, X. Zhan, M. G. Hahm, M. R. Anantharaman, G. Lawes, P. M. Ajayan, *Nano Lett.*, 2012, **12**, 3025.
- 5 D. H. Park, Y. B. Lee, M. Y. Cho, B. H. Kim, S. H. Lee, Y. K. Hong, J. Joo, H. C. Cheong, S. R. Lee, *Appl. Phys. Lett.*, 2007, **90**, 093112.
- 6 D. W. Shi, J. Y. Chen, S. Raiz, W. P. Zhou, X. F. Han, *Nanotechnology*, 2012, **23**, 305601.
- 7 H. L. Su, S. L. Tang, N. J. Tang, R. L. Wang, M. Lu, Y. W. Du, *Nanotechnology*, 2005, **16**, 2124.
- 8 Y. T. Chong, D. Gorlitz, S. Martens, M. Y. E. Yau, S. Allende, J. Bachmann, K. Nielsch, *Adv. Mater.*, 2010, **22**, 2435.
- 9 B. Daly, D. C. Arnold, J. S. Kulkarni, O. Kazakova, M. T. Shaw, S. Nikitenko, D. Erts, M. A. Morris, J. D. Holmes, *Small*, 2006, **2**, 1299.
- 10 C. Mu, Y. Yu, R. Wang, K. Wu, D. Xu, G. Guo, *Adv. Mater.*, 2004, **16**, 1550.
- 11 T. Kimura, T. Goto, H. Shintani, K. Ishizaka, T. Arima, Y. Tokura, *Nature*, 2003, **426**, 55.

- 12 N. Hur, S. Park, P. A. Sharma, J. S. Ahn, S. Guha, S. W. Cheong, *Nature*, 2004, **429**, 392.
- 13 X. J. Lou, M. Zhang, S. A. T. Redfern, J. F. Scott, *Phys. Rev. Lett.*, 2006, **97**, 177601.
- 14 G. Catalan, J. F. Scott, *Adv. Mater.*, 2009, **21**, 2463.
- 15 G. A. Solensky, V. A. Isupov, A. Agronovskaya, *Sov. Phys. Solid State*, 1959, **1**, 150.
- 16 J. Wang, J. B. Neaton, H. Zheng, N. Nagarajan, S. B. O-gale, B. Liu, D. Viehland, V. Vaithyanathan, D. G. Schlom, U. V. Waghmare, N. A. Spaldin, K. M. Rabe, M. Wuttig, R. Ramesh, *Science*, 2003, **299**, 1719.
- 17 T. J. Park, Y. Mao, S. S. Wong, *Chem. Commun.*, 2004, **23**, 2708.
- 18 X. Y. Zhang, C. W. Lai, X. Zhao, D. Y. Wang, J. Y. Dai, *Appl. Phys. Lett.*, 2005, **87**, 143102.
- 19 J. Dho, X. Qi, H. Kim, J. L. MacManus-Driscoll, M. G. Blamire, *Adv. Mater.*, 2006, **18**, 1445.
- 20 N. Dix, R. Muralidharan, J. M. Rebled, S. Estrad, F. Peir, M. Varela, J. Fontcuberta, F. Snchez, *ACS nano*, 2010, **4**, 4955.
- 21 S. Khizroev, M. H. Kryder, D. Litvinov, D. A. Thompson, *Appl. Phys. Lett.*, 2002, **81**, 2256.
- 22 A. K. Salem, P. C. Searson, K. W. Leong, *Nature Mater.*, 2003, **2**, 668.
- 23 S. Shamaila, D. P. Liu, R. Sharif, J. Y. Chen, H. R. Liu, X. F. Han, *Appl. Phys. Lett.*, 2009, **94**, 203101.
- 24 X. F. Han, S. Shamaila, R. Sharif, J. Y. Chen, H. R. Liu, D. P. Liu, *Adv. Mater.*, 2009, **21**, 4619.
- 25 R. Palai, R. S. Katiyar, H. Schmid, P. Tissot, S. J. Clark, J. Robertson, S. A. T. Redfern, G. Catalan, J. F. Scott, *Phys. Rev. B*, 2008, **77**, 014110.
- 26 G. C. Han, B. Y. Zong, P. Luo, *J. Appl. Phys.*, 2003, **93**, 9202.
- 27 S. Matt, K. Takano, S. S. P. Parkin, E. E. Fullerton, *Phys. Rev. Lett.*, 2001, **87**, 087202.
- 28 L. Sun, S. M. Zhou, P. C. Searson, C. L. Chien, *J. Appl. Phys.*, 2003, **93**, 6841.
- 29 M. P. Proenca, J. Ventura, C. T. Sousa, M. Vazquez, J. P. Araujo, *Phys. Rev. B*, 2013, **87**, 134404.
- 30 L. Liu, W. Zhou, S. Xie, L. Song, S. Luo, D. Liu, J. Shen, Z. Zhang, Y. Xiang, W. Ma, Y. Ren, C. Wang, G. Wang, *J. Phys. Chem. C*, 2008, **112**, 2256.
- 31 W. F. Brown, *Phys. Rev.*, 1963, **130**, 1677.
- 32 M. Kiwi, *J. Magn. Magn. Mater.*, 2001, **234**, 584.

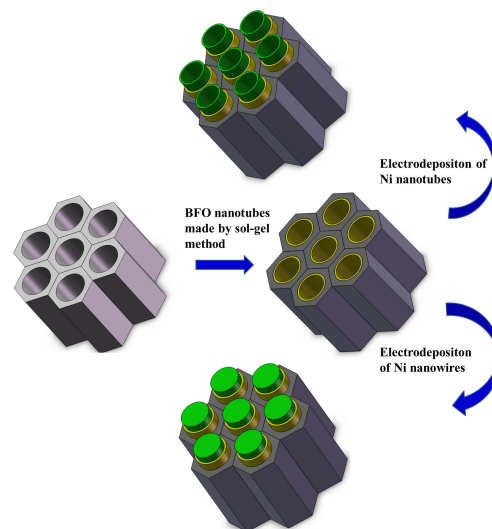


**Fig. 1** Ni-BFO core-shell nanostructures prepared via a template-assisted sol-gel and electrodeposition two step route.

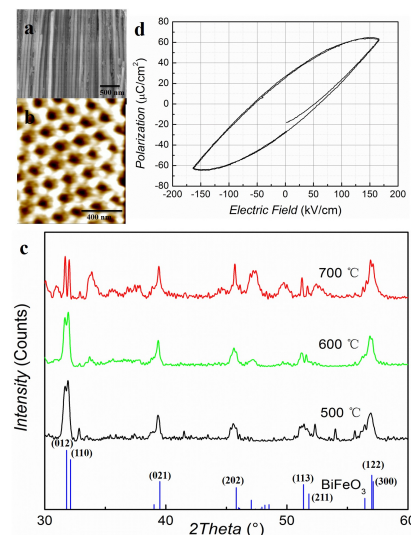


**Fig. 2** (a) Well-ordered and uniform BFO nanotubes embedded in the AAO template. (b) The surface profile of the AAO template filled with BFO nanotubes. (c) XRD patterns of the nanotubes annealed at different temperatures. (d) Ferroelectric bipolar  $P$ - $E$  hysteresis loop of the BFO nanotube arrays.

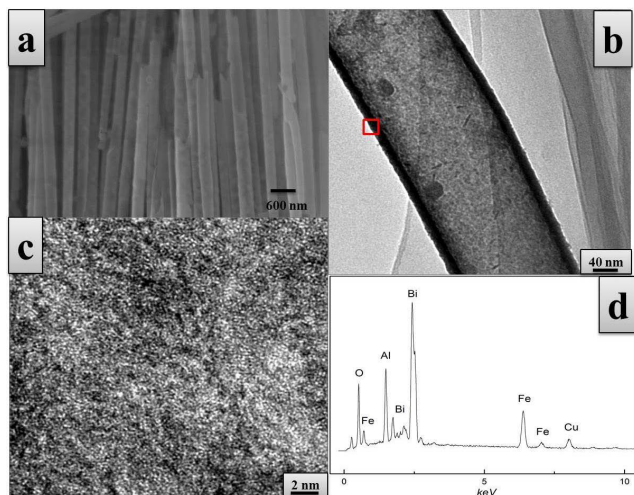


**Fig. 3** (a) SEM image of BFO nanotubes with a diameter of 300 nm. (b) TEM image of a single BFO nanotube. (c) HRTEM image shows the polycrystalline structure of BFO nanotubes. (d) Composition of the BFO nanotubes obtained from the EDS. The red mark in (b) shows the enlarge area for (c).

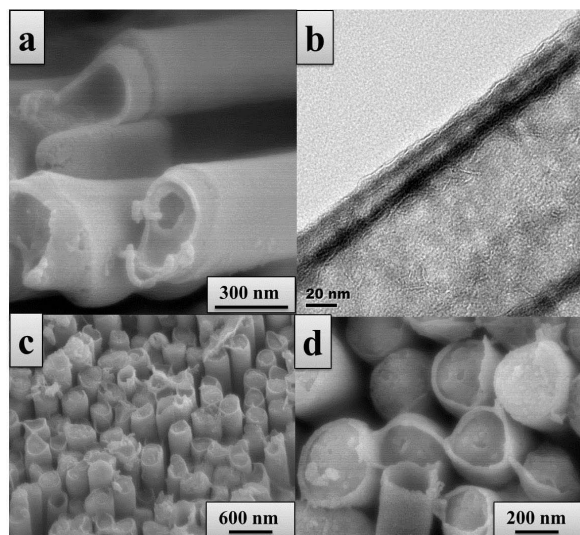


**Fig. 4** (a) SEM image of Ni-BFO core-shell nanotubes. (b) TEM image of a single Ni-BFO core-shell nanotube. (c-d) SEM images of Ni-BFO core-shell nanowires grown in AAO membranes with pore size of 300 nm.

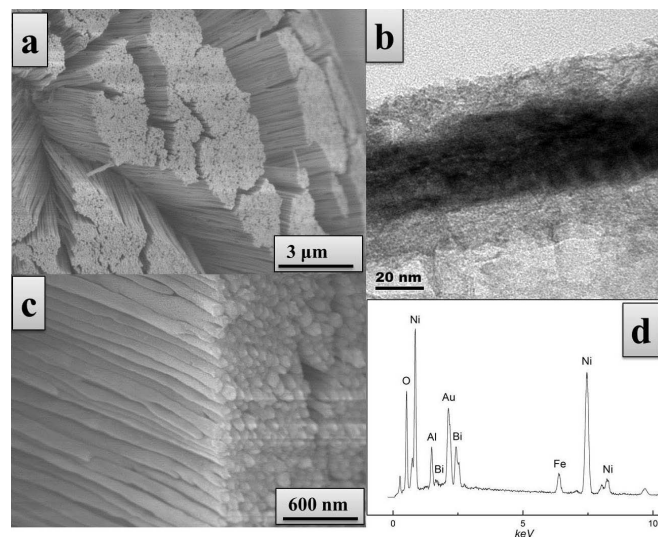


**Fig. 5** (a) SEM image of Ni-BFO core-shell nanowires with a diameter of 120 nm. (b) TEM image of a single Ni-BFO core-shell nanowire. (c) SEM image of Ni-BFO nanowires shows the core-shell structure. (d) Composition of the Ni-BFO core-shell nanowires got from EDS.

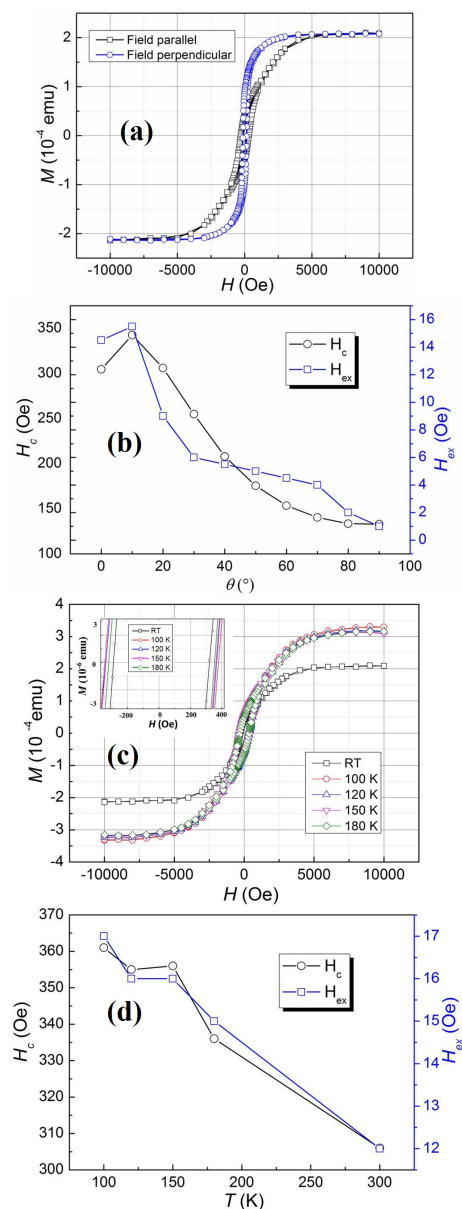


**Fig. 6** (a) Hysteresis loops of Ni-BFO core-shell nanotubes for magnetic fields applied parallel and perpendicular to the nanotube axis. (b) The angular dependence of coercivity and exchange bias field of Ni-BFO core-shell nanotubes. (c) Hysteresis loops of Ni-BFO core-shell nanotubes at different temperatures. (d) Temperature dependence of the coercivity and exchange bias field.

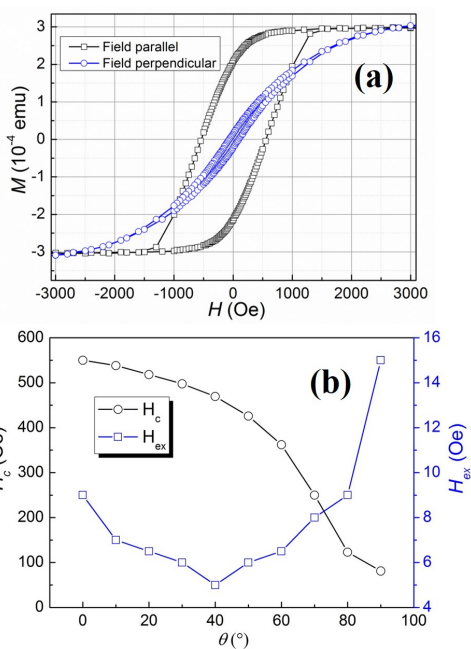


**Fig. 7** (a) Hysteresis loops of Ni-BFO core-shell nanowires (120 nm) for magnetic fields applied parallel and perpendicular to the nanowire axis at room temperature. (b) Angular dependence of the coercivity and exchange bias field.